Zero-temperature phase diagram of mixed-stack charge-transfer crystals

A. Painelli
Department of Physical Chemistry, University of Padua, 2 via Loredan, I-35131 Padua, Italy

A. Girlando
Institute of Physical Chemistry, University of Parma, via delle Scienze, I-43100 Parma, Italy
(Received 14 August 1987)

The zero-temperature phase diagram of mixed-stack charge-transfer crystals is investigated through a diagrammatic valence-bond technique. The direct solution of the single-chain Hubbard Hamiltonian inclusive of intersite Coulomb interactions constitutes the basis for a perturbative, adiabatic treatment of the electron–lattice-phonon and electron–molecular-vibration couplings. It is shown that intersite Coulomb interactions and electron–molecular-vibration coupling cooperate in favoring uneven distribution of the electronic charge on the sites, possibly giving rise to a discontinuous, first-order neutral-ionic (*N-I*) phase transition. On the other hand, the electron–lattice-phonon coupling favors an uneven distribution of the charge between the sites, yielding a Peierls-type dimerization instability. However, when all the interactions are turned on, a rather subtle feedback interplay is found, the dimerization instability range being widened by the Coulomb interactions and the electron–molecular-vibration coupling. The resulting four-dimensional phase diagram is able to account for the experimentally observed ground states and phase transitions of mixed-stack charge-transfer crystals. In particular, it is found that the boundary between *N* regular stack phases and *I* dimerized ones is, in general, very complex, as several minima in the potential-energy curve are available to the system. Consequently, the corresponding phase transition is very sensitive to the experimental conditions, a situation we believe is encountered in the famous *N-I* transition of tetrathiafulvalene-chloranil. In addition, preliminary calculations on dimerized stack systems show that whereas ionic regular chains are intrinsically unstable towards dimerization, the corresponding energy gain decreases as the ionicity increases. Therefore at finite temperatures ionic regular stacks may be observed, their transition temperature to the dimerized phase being expected to be lower with increasing ionicity.

I. INTRODUCTION

Organic mixed-stack charge-transfer (CT) crystals are made up by chains of alternating electron-donor (*D*) and -acceptor (*A*) molecules, $\cdots A^{\rho-}D^{\rho+}A^{\rho-}D^{\rho+}\cdots$, ρ being the degree of ionicity (sometimes referred to as the average degree of CT along the stack).[1] Since the discovery of pressure[2]- or temperature[3]-induced phase transitions implying a change in ionicity (neutral-ionic, *N-I*, phase transitions), many experimental investigations have been carried out,[4–6] and a number of theoretical models have been proposed[7–14] aimed at understanding this new kind of transition. On the experimental side it has been recognized that the *N-I* transition is a quite uncommon and complex event:[15] it has in fact been clearly identified only for the tetrathiafulvalene-chloranil (TTF-CA) crystal, and in such a case it is accompanied by a stack dimerization.[4–6] Moreover other types of phase transitions have been observed, involving only the stack dimerization[15,16] (i.e., *Nr-Nd* and *Ir-Id*; *r* and *d* stand for regular and dimerized stack, respectively).

The proposed theoretical models clearly point out that the stability of the four observed phases (*Nr*, *Nd*, *Ir*, *Id*) in mixed-stack CT crystals is determined by the interplay between electrostatic intersite interactions (we shall refer to them as Coul interactions) and the electron–lattice-phonon (*e*–lph) coupling. Both these interactions couple to the electronic density; in particular, the *e*-lph coupling, favoring an uneven electronic distribution between the molecular sites (bond order wave BOW), leads to a stabilization of dimerized structures. On the contrary, the Coul interactions couple to the site-electron-density wave (SEW): they favor an uneven distribution on the molecular sites of the electron exchanged between *D* and *A* molecules,[17] possibly causing a discontinuous ionicity variation in going from *N* to *I* regime. However, as we have pointed out in a preliminary paper,[13] there is a third kind of interaction which affects the properties of mixed-stack CT crystals: the electron–molecular vibration (*e*-mv) one, which, having the same symmetry as the Coul interactions, also couples with the SEW. None of the previously proposed models[7–12,14] has simultaneously taken into account all the above interactions.

The valence bond (VB) technique has proven to be a valuable numerical method to describe the properties of mixed-stack CT crystals.[18] Besides the advantage of working with basis functions (the electronic configurations) which are well known in the field of physical chemistry, the VB method allows one to easily treat the Coul interactions, being not limited to mean-field (mf) ap-

proximation, nor to nearest-neighbor interactions.[9,19] In a previous paper[11] (hereafter paper I) we have applied the VB technique in a first description of the interplay between *N-I* and *r-d* interfaces, treating the Coul interactions in mf approximation and introducing the *e*-lph coupling via a perturbative approach. Here we extend the analysis by relaxing the mf approximation (an unscreened Coulomb potential will be considered), and by introducing also the *e*-mv coupling. In this way we are able to draw the complete zero-temperature phase diagram of mixed-stack CT crystals. Although some of the results have already been anticipated,[13] the consequences of the rather subtle interplay between the various types of interactions were not analyzed in detail. Moreover in this paper we correct a previous misconception,[11,13] showing that at 0 K the *Ir* phase is intrinsically unstable towards dimerization.

The paper is organized as follows. The next two sections introduce the model and analyze the ground-state properties of the system in the absence of electron-phonon coupling. Section IV introduces the *e*-mv coupling and its consequences on the *N-I* instability, whereas in Sec. V we treat the consequences of *e*-lph coupling. Section VI reports the full phase diagram, expressed in terms of experimentally accessible parameters. Before drawing the conclusions, the comparison of the phase diagram with the experimental data is carried out, and a brief outline of the temperature effect is given.

II. ELECTRONIC HAMILTONIAN

The properties of mixed-regular-stack CT crystals are investigated by choosing as a model system an isolated DA regular chain, with one Wannier orbital per molecular site and with only the nearest-neighbor CT integral different from zero (t, defined positive). We also exclude the states with doubly ionized molecular sites (D^{++} and A^{--}) by assuming a large value for the on-site electrostatic interactions (the Hubbard U), i.e., $U/t \to \infty$ for both D and A molecules.[19] Estimates of U for several D and A molecules indeed place it in the 4–7 eV range;[20] since typical values of t in mixed-stack CT crystals are 0.1–0.4 eV (Ref. 21), $U/t \sim 10$–70. The large-U assumption is therefore a sensible one, and the purely electronic Hamiltonian is written as (here and henceforth $\sqrt{2}t=1$ and $\hbar=1$):

$$\mathcal{H}=-\delta_0\sum_i(-1)^i n_i-\sqrt{2}\sum_i b_i+\sum_{\substack{i,j\\(i>j)}}V_{ij}\hat{\rho}_i\hat{\rho}_j\ , \qquad (1)$$

where i counts the $\mathcal{N}$ molecular sites (odd for D and even for A) and σ the two spin states (α,β).

$$n_i=\sum_\sigma a_{i,\sigma}^\dagger a_{i,\sigma}$$

and

$$b_i=2^{-1}\sum_\sigma(a_{i,\sigma}^\dagger a_{i+1,\sigma}+\text{H.c.})$$

are the occupation number and bond order operators, respectively, $a_{i,\sigma}^\dagger$ ($a_{i,\sigma}$) being the Fermi creation (annihilation) operator of an electron with spin σ at the ith site. If one assimilates the Wannier orbitals with the molecular ones, $2\delta_0=A_A-I_D$, where A_A and I_D are the electron affinity of A and the ionization potential of D, respectively. The last term in Eq. (1) accounts for the intersite electronic interactions, V_{ij} being the interaction energy between fully ionic i and j sites, and $\hat{\rho}_i$ the charge operator defined as $\hat{\rho}_i=2-n_i$ at D sites and $\hat{\rho}_i=n_i$ at A ones.

The large-U assumption embedded in Eq. (1) Hamiltonian has been generally adopted in the description of mixed-stack CT crystals.[7–9,11,14] Only Nagaosa[12] (and, apparently, Luty[10]) assumes a rather small-U value ($U=1.5$ eV), corresponding to an effective value screened by electron-electron interaction and which cannot be introduced in a Hamiltonian where these interactions are explicitly accounted for.[22] Since Nagaosa's Hamiltonian reduces to that of Eq. (1) only in the large-U limit, his model is actually different from the other ones.

The Eq. (1) Hamiltonian can be solved by treating the Coul interactions in mf approximation, i.e., by substituting one of the two $\hat{\rho}$ operators in the last term with its ground-state mean value ($\rho=\langle\hat{\rho}\rangle$).[23] In order to get a proper estimate of the pair ionization energy for any value of the ground-state ionicity, the average is performed as follows:

$$\tfrac{1}{2}\left\langle{\sum_j}'V_{ij}\hat{\rho}_j\right\rangle=-V[1+2\rho(\alpha-1)]\ , \qquad (2)$$

where V is the absolute value of the electrostatic interaction between fully ionic nearest-neighbor sites and α an effective Madelung constant defined by $\mathcal{N}V\alpha=-\sum'_{i,j}V_{ij}$. The mf approach can, therefore, be applied irrespective of the specific form of the electrostatic potential, provided α is finite. In particular, for an infinite stack α ranges from 2, when only nearest-neighbor interactions are present, to $2\ln 2$ when an unscreened, long-range Coulomb (lr-Coul) potential is introduced.[9] In any case the Hamiltonian in Eq. (1) simplifies as follows:

$$\mathcal{H}=-z\sum_i(-1)^i n_i-\sqrt{2}\sum_i b_i\ . \qquad (3)$$

The electronic Hamiltonian in mf approximation depends explicitly only on the z parameter, which represents half of the energy required to destroy an ionic pair in a stack with ionicity ρ:

$$z=z_0+\varepsilon_c\rho\ , \qquad (4)$$

where $z_0=\delta_0+V/2$ and $\varepsilon_c=V(\alpha-1)$. In paper I the Hamiltonian in Eq. (3) has been solved and the ground-state properties and the stability of the system have been investigated. A self-consistent approach has then been applied to study the effects of finite ε_c values on the system ionicity.

In this paper we shall directly solve the full Hamiltonian in Eq. (1), choosing as electrostatic potential a lr-Coul one, i.e., by setting

$$V_{ij}=\pm V/d_{ij}\ , \qquad (5)$$

where d_{ij} is the distance between i and j sites (in units of the nearest-neighbor intermolecular distance) and the plus sign applies when i and j are both odd or both even, the minus otherwise. Also in this case the two parame-

TABLE I. Madelung constants adopted in the valence-bond (VB) calculations of finite mixed-stack systems.

$\mathcal{N}$	α_{rings}	α_{chains}
4	1.292 89	1.166 67
6	1.345 30	1.233 33
8	1.363 35	1.269 05
10	1.371 65	1.291 27
12	1.376 14	1.306 42
14	1.378 84	
∞	1.386 29	1.386 29

ters z_0 and ε_c [Eq. (4)] can be defined, α being the usual Madelung constant. The Hamiltonian is solved for finite rings and open chains adopting the α values reported in Table I (they properly converge to 2 ln2 limit as $\mathcal{N}\rightarrow\infty$). The results for the infinite stack are obtained through the extrapolation procedure previously described.[11]

III. GROUND STATE IN THE ABSENCE OF ELECTRON-PHONON COUPLING: EFFECT OF ELECTROSTATIC INTERACTIONS

We have already shown[11] that finite size rings (point group $C_{\mathcal{N}/2,v}$) behave in a very different way depending on the $\mathcal{N}/2$ value. In odd rings ($\mathcal{N}/2$ odd) the ground state belongs always to the A_1 representation (i.e., it is symmetric in respect to translation and reflection), whereas in even rings ($\mathcal{N}/2$ even) for z exceeding some critical value, the ground state becomes antisymmetric in respect to reflection (A_2 representation). These results were obtained for uncorrelated ($\varepsilon_c=0$) rings; the present lr-Coul calculations yield the same picture also for $\varepsilon_c\neq 0$, as shown in Fig. 1 where we report the energy per site (measured as difference from the energy of the fully ionic ring) of the lowest A_1 and A_2 singlets calculated as a function of z_0 for an odd ring ($\mathcal{N}=6$) and for an even one ($\mathcal{N}=8$) with various ε_c values. It is, therefore, not surprising that also the corresponding singlet-singlet energy gap (Δ_{ss}) behaves in a similar way in uncorrelated and correlated infinite stacks. This is shown in Fig. 2, where the $\Delta_{ss}(z_0)$ curves obtained by lr-Coul calculations are reported: for each ε_c there is a critical z_0 value, z_0^*, above which Δ_{ss} vanishes. The physical origin of the ground-state degeneracy found for $z_0>z_0^*$ has been extensively discussed in paper I. We only remind that the nondegenerate ($z_0<z_0^*$) regime can be described as a "neutral" one, i.e., a regime where fully ionic diagrams do not contribute to the ground state, whereas the degenerate ($z_0>z_0^*$) regime is an "ionic" one, where no contribution from the fully neutral diagram is found in the ground state.

From Fig. 2 data we estimate the $z_0^*(\varepsilon_c)$ values, as done in paper I for the uncorrelated stack. The results are collected in the first column of Table II, together with the corresponding mf values, obtained through the relation $z_0^*(\varepsilon_c)=z_c-\varepsilon_c\rho_c$, where $z_c=z_0^*(0)$ and $\rho_c\sim 0.63$ is the ionicity of the uncorrelated stack at z_c.[11] In the same table we report the corresponding data from Ref. 9: the

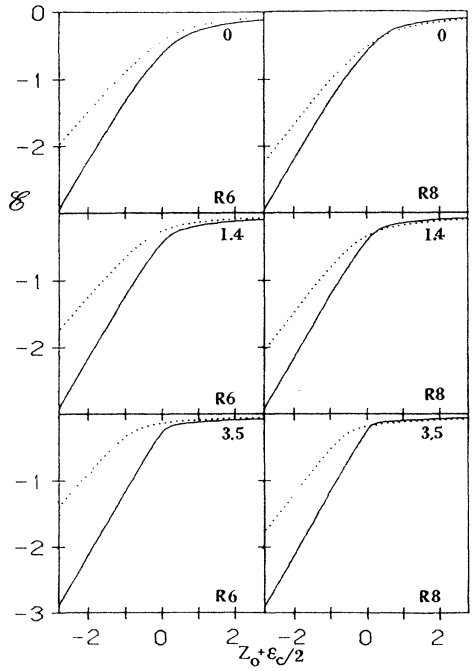

FIG. 1. Energy per site ($\mathscr{E}$) of $\mathcal{N}=6$ and 8 DA rings (R), as a function of $z_0+\varepsilon_c/2$ and for various ε_c values (marked in the upper left corner of each panel). The results refer to lr-Coul calculations. Solid line: lowest energy A_1 singlet; dotted line: lowest energy A_2 singlet.

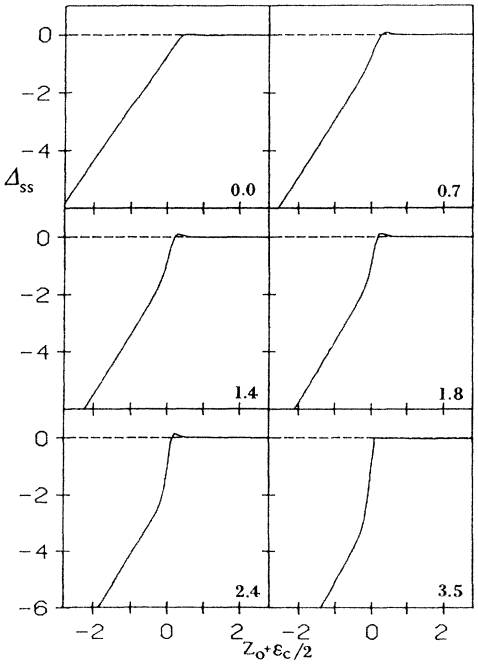

FIG. 2. Singlet-singlet energy gap (Δ_{ss}) of the infinite DA chain obtained by lr-Coul calculations for various ε_c values (marked in the bottom left corner of each panel).

overall agreement between the three sets of data gives us confidence in the obtained results. In particular it turns out that the mf approach leads to sensible results at least for not too large ε_c values ($\varepsilon_c \lesssim 3.5$). We observe that by increasing ε_c, the *N-I* boundary shifts towards lower $z_0+\varepsilon_c/2$ values and becomes more and more steep (Fig. 2), suggesting the presence of highly unstable states at intermediate ionicity (the SEW is favored by Coul interactions). This result is consistent with the analytic one obtained in the $\varepsilon_c \to \infty$ limit ($t \to 0$), where the chain is found to be unstable for $0<\rho<1$, the boundary occurring at $I_D - A_A = V\alpha$, i.e., at $z_0+\varepsilon_c/2=0$.[24]

In Fig. 3 we report, as a function of z_0, the ground-state energy per site ($\mathcal{E}_G$) calculated by the lr-Coul approach for the infinite stack at various ε_c values. Also in this case the *N-I* boundary, which can be identified as the region where the curves change slope, is found to occur at lower $z_0+\varepsilon_c/2$ values as ε_c increases and at the same time to become steeper. The curves in Fig. 3 allow us to evaluate, without further calculations, the ground-state ionicity of the system. In fact, by applying the Hellmann-Feynmann theorem to the Eq. (1) Hamiltonian, one has[23]

$$\rho = 1 - \frac{\partial \mathcal{E}_G}{\partial z_0} , \tag{6}$$

where the derivatives are evaluated at constant ε_c. The $\rho(z_0)$ curves at various ε_c values are reported in Fig. 4, together with the mf results.[11] Since the $\mathcal{E}_G(z_0)$ curves (Fig. 3) change abruptly their slope from ~ 1 to ~ 0 at $z_0 \sim z_0^*$, one correspondingly finds a steep ρ variation from *N* to *I* values, supporting our interpretation of the nondegenerate ($z_0 < z_0^*$) and degenerate ($z_0 > z_0^*$) regimes

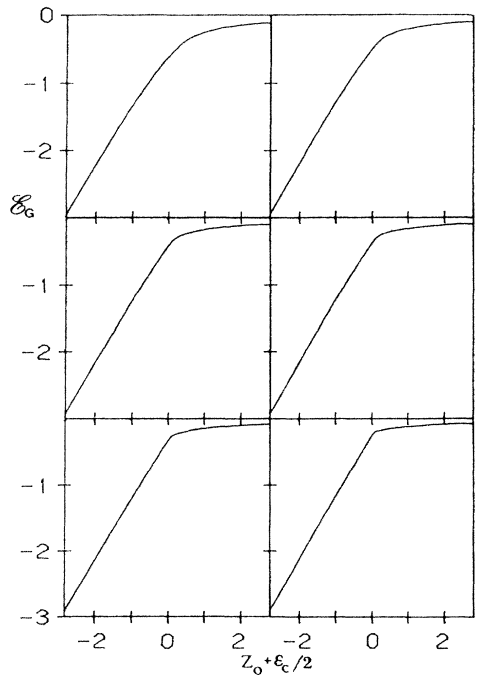

FIG. 3. Ground-state energy ($\mathcal{E}_G$) of the infinite *DA* chain obtained by lr-Coul calculations for the same ε_c values as Fig. 2.

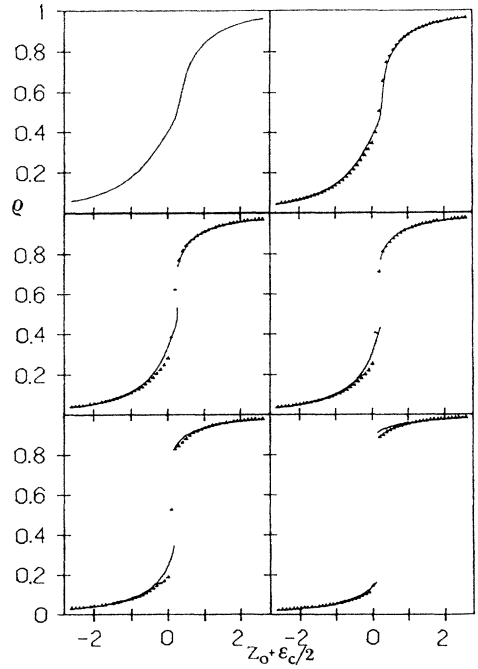

FIG. 4. Effect of ε_c on the degree of ionicity (ρ) as a function of $z_0+\varepsilon_c/2$. The ε_c values are the same as Fig. 2. Lines and triangles refer to mf and lr-Coul calculations, respectively.

as *N* and *I* ones. Moreover, it is seen that for ε_c greater than a critical value (about 1.8–2.4) the slope variation in the $\mathcal{E}_G(z_0)$ curves becomes so abrupt as to originate a finite difference in the left and right derivatives at z_0^*, suggesting the presence of a sudden, first-order phase transition. This result agrees with the mf picture,[11] where the self-consistent solution of the Eq. (3) Hamiltonian at large ε_c values leads to the appearance of forbidden ionicity regions. However, due to the large uncertainties introduced by the differentiation process, the *N-I* interface will be better analyzed in the next section, where we introduce the effect of *e*-mv coupling.

IV. *e*-mv COUPLING AND *N-I* INSTABILITY

We shall now investigate the effects of the electron-phonon coupling on the solution of the purely electronic Hamiltonian described in the previous section. We first consider the phonons able to modulate the on-site energies (I_D and A_A), i.e., the *D* and *A* vibrations belonging to the totally symmetric representation of the respective molecular point group.[25] Such a modulation is responsible for the coupling between electronic and molecular degrees of freedom and is generally referred as electron-molecular vibration (*e*-mv) coupling. In a previous paper[25] we have shown that the interesting physics of *e*-mv coupling can be described by expanding the electronic Hamiltonian at the first order in the vibrational coordinates, i.e., by introducing the following *e*-mv Hamiltonian:

$$\mathcal{H}_{ev} = \mathcal{N}^{-1/2} \sum_i (-1)^i n_i \sum_\gamma \sqrt{\omega_\gamma} g_\gamma Q_\gamma , \tag{7}$$

where i counts the molecular sites and γ the totally symmetric vibrations of D and A molecules, g_γ being the corresponding coupling constant as usually defined.[25] Q_γ and ω_γ are the equilibrium crystal normal coordinates (at $k=0$) and the vibrational frequencies, respectively; the purely vibrational Hamiltonian obviously is

$$\mathcal{H}_v = 2^{-1} \sum_\gamma (\dot{Q}_\gamma^2 + \omega_\gamma^2 Q_\gamma^2) .$$

Since the perturbing Hamiltonian in Eq. (7) retains the reflection symmetry of the electronic Hamiltonian, we expect that the e-mv interaction couples to the SEW and that its contribution adds to that of ε_c in setting up the on-site charge distribution.

The consequences of e-mv coupling on the vibrational spectra of CT crystals have already been extensively investigated.[21,25] In particular we have shown that for a mixed-regular-stack system this coupling induces a shift (generally a lowering) of the frequencies of the totally symmetric molecular modes in respect to their unperturbed values. The squares of the perturbed frequencies are found by diagonalizing the force constant matrix (F), whose elements are given by

$$F_{\gamma\gamma'} = \omega_\gamma^2 \delta_{\gamma\gamma'} - \chi_v \sqrt{\omega_\gamma \omega_{\gamma'}}\, g_\gamma g_{\gamma'} , \tag{8}$$

where $\delta_{\gamma\gamma'}$ is the Krönecker δ and χ_v the electronic response to the e-mv perturbation:

$$\chi_v = \frac{2}{\mathcal{N}} \sum_F \frac{|\langle G | \sum_i (-1)^i n_i | F \rangle|^2}{\omega_F} , \tag{9}$$

$|G\rangle$ and $|F\rangle$ being the ground and excited electronic states and ω_F the frequency of the $|F\rangle \rightarrow |G\rangle$ transition.

In a previous paper[21] we have analyzed the consequences of Eq. (8) in the hypothesis that the system is stable in respect to molecular distortions. On the other hand, if the e-mv perturbation is strong enough, the F matrix has negative eiegenvalues: the corresponding modes (proper combinations of the Q_γ's) become, therefore, unstable in respect of a relaxation to a new equilibrium position. Since the equilibrium Q_γ's are intrinsically related to the molecular charge,[25] the coordinate relaxation actually implies a charge redistribution between D and A molecules. The region where some of the F eigenvalues become negative, therefore, corresponds to a forbidden ionicity region, the instability condition being given by

$$\varepsilon_{sp} \geq \chi_v^{-1} , \tag{10}$$

where $\varepsilon_{sp} = \sum_\gamma g_\gamma^2 / \omega_\gamma$ is the small-polaron binding energy, the gain in electronic energy (per unit cell) due to the relaxation of the molecular coordinates when the charge of the system changes from 0 to 1.[13]

The $\chi_v^{-1}(\rho, \varepsilon_c)$ curves already obtained[21] through mf and lr-Coul calculations, and here reported in Fig. 5, can, therefore, be interpreted as phase diagrams for the N-I instability: putting on the ordinate axis the ε_{sp} values, the only stable states of a given system are those described by the points lying below the corresponding χ_v^{-1} curve.

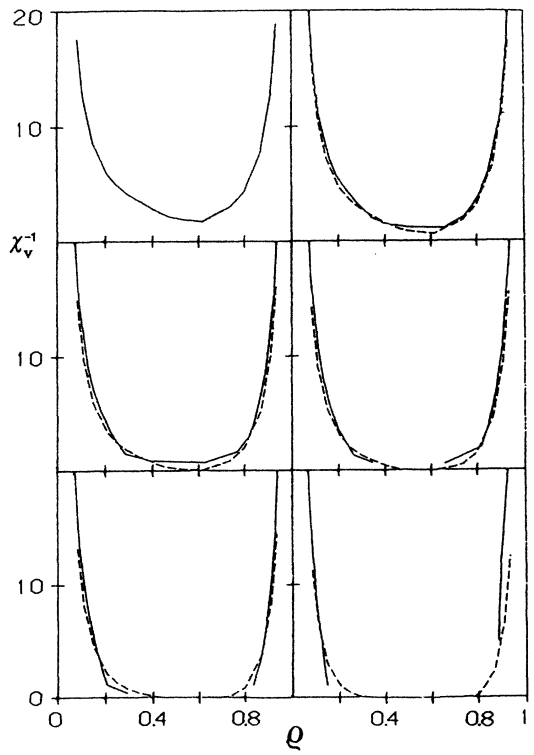

FIG. 5. Inverse of the electronic response of the e-mv perturbation (χ_v) as a function of ρ for different ε_c values (the same as Fig. 2). Dashed and solid lines refer to mf and lr-Coul calculations, respectively,

These phase diagrams can also give information on the N-I instability in the absence of e-mv coupling ($\varepsilon_{sp}=0$). In such a case the allowed ρ values are those where χ_v^{-1} is a positive, finite quantity. The information is, of course, the same as that conveyed by the $\rho(z_0)$ curves (Fig. 4), but the borderline of the allowed ionicity regions is more precisely defined. In particular in Table II we report the corresponding z_0^* values: they compare well with those obtained in the previous section. Moreover we estimate $\varepsilon_c^* \sim 2.0$, in good agreement with Soos' result.[9]

Coming back to the most general case of a finite ε_{sp} value, one has to consider the proper ε_{sp}=constant line, searching for its possible intersections with the $\chi_v^{-1}(\rho, \varepsilon_c)$ curve. As an example consider a system with $\varepsilon_c = 0.7$ (upper right panel): for $\varepsilon_{sp} \lesssim 1$ the N-I interface is continuous, any ρ value being allowed; otherwise an instabili-

TABLE II. Neutral-ionic boundary ($z_0^* + \varepsilon_c/2$) for mixed regular stacks, as a function of the Coul interaction energy (ε_c).

	From Δ_{ss} curves		From χ_v^{-1} curves		
ε_c	lr-Coul	mf	lr-Coul	mf	Ref. 9
0.00	0.42	0.42	0.38	0.38	
0.71	0.26	0.33	0.29	0.31	
1.41	0.20	0.24	0.19	0.24	0.21
1.77	0.18	0.19	0.19	0.20	0.17
2.36	0.14	0.11	0.10	0.14	0.13
3.54	0.09	−0.04	0.10	0.03	0.09

ty range opens up, e.g., at $\varepsilon_{sp}=2$ the states with ionicity in between $\rho_N \sim 0.34$ and $\rho_I \sim 0.73$ are not stable. On the other hand, when $\varepsilon_c > \varepsilon_c^*$ the N-I interface is always discontinuous, e.g., if $\varepsilon_c=2.4$ at $\varepsilon_{sp}=0$, $\rho_N \sim 0.35$ and $\rho_I \sim 0.80$; at $\varepsilon_{sp}=2.0$, $\rho_N \sim 0.19$ and $\rho_I \sim 0.82$. Thus both ε_c and ε_{sp} contribute to widen the charge instability region, favoring the SEW formation; in other terms, by increasing ε_c and/or ε_{sp} the $\rho_I - \rho_N$ difference becomes more and more large.

In order to get a better insight into the role played by the e-mv coupling in the N-I instability and a better description of the corresponding phase transition, we shall now approach the problem from a different side. From the total Hamiltonian (sum of the lr-Coul electronic, the e-mv, and the purely vibrational ones) it is easy to get the equations of motion for the Q's and evaluate their equilibrium position in the ground state:

$$\langle Q_\gamma \rangle = \mathcal{N}^{1/2}(1-\rho)\omega_\gamma^{-3/2} g_\gamma \ . \tag{11}$$

In the adiabatic limit this ground-state expectation value can be substituted in the e-mv Hamiltonian [Eq. (7)] to give

$$\mathcal{H}_{ev} = (1-\rho)\varepsilon_{sp} \sum_i (-1)^i n_i \ . \tag{12}$$

Following the same reasoning adopted in the mf treatment of the electronic correlations,[11,23] this Hamiltonian can be absorbed in the purely electronic one [Eq. (1)] by a renormalization of z_0:

$$\zeta = z_0 - \varepsilon_{sp}(1-\rho) \ . \tag{13}$$

The problem has a self-consistent solution: from the known $\rho(z_0, \varepsilon_c, \varepsilon_{sp}=0)=\rho(\zeta, \varepsilon_c)$ curves (Fig. 4) one can evaluate $z_0=\zeta+\varepsilon_{sp}(1-\rho)$ for each ε_{sp} and then construct the $\rho(z_0, \varepsilon_c, \varepsilon_{sp})$ curves. Examples of the resulting curves are reported in Fig. 6 for a system with $\varepsilon_c=1.8$ and different values of ε_{sp}.

By increasing ε_{sp}, the $\rho(z_0)$ curve becomes more and more steep, and when its slope becomes negative, the system is driven into an instability region. It is not difficult to realize that the stability condition $(\partial\rho/\partial z_0)>0$ (equivalent to $\partial^2 \mathcal{E}_G/\partial\rho^2>0$) (Ref. 11) actually reduces to the condition reported in Eq. (10). The effect of ε_{sp} on the N-I interface is strictly analogous to that of ε_c: the S-shaped $\rho(z_0)$ curves occurring for sufficiently large ε_c and ε_{sp} values clearly indicate the presence of a first-order N-I phase transition characterized by a bistability region where two stable states $(\partial\rho/\partial z_0>0)$ coexist with an unstable one $(\partial\rho/\partial z_0<0)$.[26]

If one wants to apply the same procedure to the mf solution of the electronic Hamiltonian, some problems arise. In fact, as it has been shown in a previous paper,[21] in such a case the e-mv Hamiltonian has to be multiplied by the $[1-\varepsilon_c\chi_v(\rho, \varepsilon_c=0)]^{-1}$ factor. Then it can be included in the electronic Hamiltonian [Eq. (3)] by simply renormalizing z to

$$\zeta = z - \frac{\varepsilon_{sp}(1-\rho)}{1-\varepsilon_c\chi_v(\rho, \varepsilon_c=0)} = (z_0)_{eff} + \varepsilon_{eff}\rho \ ,$$

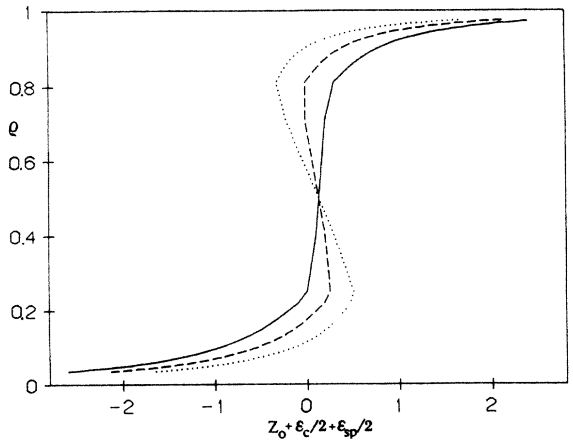

FIG. 6. Degree of ionicity (ρ) vs $z_0+\varepsilon_c/2+\varepsilon_{sp}/2$ for three ε_{sp} values (0.0, 1.0, and 2.0, indicated by solid, dashed, and dotted lines, respectively) and $\varepsilon_c=1.8$ (lr-Coul calculations).

where

$$(z_0)_{eff} = z_0 - \varepsilon_{sp}/[1-\varepsilon_c\chi_v(\rho, \varepsilon_c=0)] \ ,$$

$$\varepsilon_{eff} = \varepsilon_c + \varepsilon_{sp}/[1-\varepsilon_c\chi_v(\rho, \varepsilon_c=0)] \ .$$

Thus in this case ε_{eff} actually depends on ρ through the $\chi_v(\rho, \varepsilon_c=0)$ function; the stability of the system cannot be investigated following the usual treatment[26] since the energy derivatives in respect to $(z_0)_{eff}$ at ε_{eff} constant cannot be evaluated. For this reason, in the following we shall always adopt the lr-Coul description of the N-I instability.

V. e-lph COUPLING AND r-d STACK INSTABILITY

We now consider a second type of coupling between electronic and nuclear degrees of freedom, i.e., that produced by the modulation of CT integrals by phonons. The largest modulations are in general related to lattice phonons (from which the name of e-lph coupling) which are expected to induce the largest variations of intermolecular distances and/or angles. Also molecular modes can give rise to such a kind of coupling, but their contribution can generally be neglected. In the following we shall limit our attention to the $k=0$ modes, as they are the modes responsible for the stack dimerization (BOW formation).[11] It is also worth explicitly observing that the modes (U_ν) able to modulate t are in general also able to modulate the V_{ij}'s which appear in the last term of Eq. (1). On the other hand, due to the high symmetry of the electrostatic potential in a mixed regular chain, this modulation introduces a perturbative Hamiltonian which is quadratic in the U_ν's. The corresponding first-order correction to the energy, also quadratic in the U_ν's, leads only to a renormalization of the unperturbed frequences. The second-order correction, accounting for the mixing of different electronic functions, is usually responsible for the so-called "vibronic effects,"[25] but in this case is quartic in the U_ν's and can, therefore, be neglected in the harmonic approximation. As a consequence, by expanding the electronic Hamiltonian [Eq. (1)] to the first

order in the U_ν's, one obtains the usual e-lph Hamiltonian:[11]

$$\mathcal{H}_{ep} = -2\mathcal{N}^{-1/2} \sum_i (-1)^i b_i \sum_\nu \sqrt{\omega_\nu} g_\nu U_\nu \ , \tag{14}$$

where i counts the $\mathcal{N}$ molecular sites, ν the $k=0$ modes able to modulate t, g_ν being the corresponding coupling constants as defined in paper I. U_ν and ω_ν are the crystal equilibrium normal coordinates and frequencies, respectively, the purely vibrational Hamiltonian being $\mathcal{H}_v = 2^{-1} \sum_\nu (\dot{U}_\nu^2 + \omega_\nu^2 U_\nu^2)$. As already reported in paper I and analogously to the e-mv coupling case, the e-lph coupling leads to a shift (in general a lowering) of the frequencies of the involved modes. The squares of the perturbed frequencies are the eigenvalues of the force constant matrix (**F**), whose elements are

$$F_{\nu\nu'} = \omega_\nu^2 \delta_{\nu\nu'} - \chi_b \sqrt{\omega_\nu \omega_{\nu'}} g_\nu g_{\nu'} \ , \tag{15}$$

where χ_b is the electronic response to the e-lph perturbation (in order to simplify the notation, the following χ_b definition differs by an $\mathcal{N}$ factor from that of paper I):

$$\chi_b = \frac{8}{\mathcal{N}} \sum_F \frac{|\langle G | \sum_i (-1)^i b_i | F \rangle|^2}{\omega_F} \ . \tag{16}$$

If the e-lph perturbation is strong enough, the softening of the U_ν's described by Eq. (15) yields a lattice relaxation, i.e., a stack dimerization. This happens when one of the eigenvalues of **F** becomes negative, the unstable states being characterized by the following condition:

$$\varepsilon_d \geq \chi_b^{-1} \ , \tag{17}$$

where $\varepsilon_d = \sum_\nu g_\nu^2 / \omega_\nu$, the lattice distortion energy, measures the electronic energy gain (per unit cell) due to the relaxation of the U_ν modes when the electronic density on the bonds changes from that relevant to a regular chain to that of a fully dimerized stack.

The phase diagram for the r-d stack instability is, therefore, given by the $\chi_b^{-1}(\rho, \varepsilon_c)$ curves reported in Fig. 7: the states stable in respect to dimerization correspond to the points lying below the χ_b^{-1} curve. The $\varepsilon_c = 0$ diagram differs from that previously reported: in the I regime χ_b^{-1} is always zero, whereas small but finite values were assigned to it in paper I. The trouble comes from extrapolation procedures. In paper I the χ_b^{-1} evaluation for finite systems has been performed by choosing as $|G\rangle$ a state [Eq. (16)] with the lowest energy, i.e., for even rings in the ionic regime, an A_2 state. This choice, in principle correct, yields a very slow convergence and large uncertainties in the extrapolated values. Due to the degeneracy of the lowest A_1 and A_2 singlet states of the infinite stack in the ionic regime, it is also possible to choose as $|G\rangle$ a state with the lowest energy state in the A_1 subspace: in such a way even rings in the ionic regime are characterized by negative χ_b^{-1} values. By increasing $\mathcal{N}$ one finds that in the I regime the results for odd rings and open chains and those for even rings tend to zero from positive and negative values, respectively. Even if the convergence is not faster than above, it is not difficult to realize that χ_b^{-1} vanishes in the $N \to \infty$ limit.

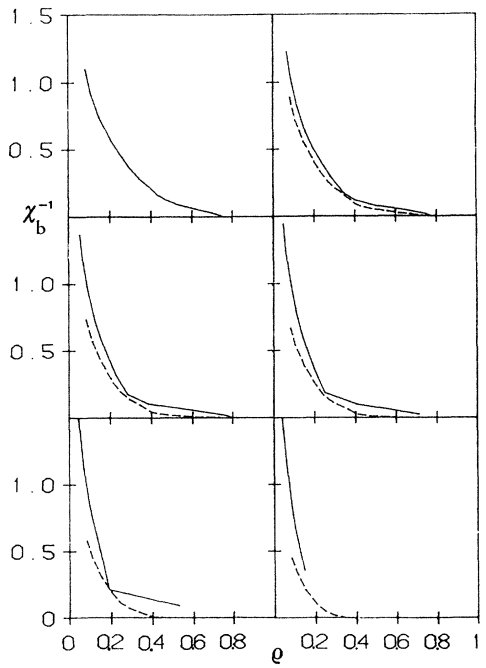

FIG. 7. Inverse of the electronic response to the e-lph perturbation (χ_b) as a function of ρ for different ε_c values (the same as Fig. 2). Dashed and solid lines refer to mf and lr-Coul calculations, respectively.

Therefore mixed regular stacks in the I regime are, at zero temperature, intrinsically unstable towards dimerization, as already recognized by Nagaosa.[12] However, as discussed in paper I, physical intuition suggests an increase of the stability of the regular stack for large-ρ values ($\rho \to 1$). This point will be discussed in Sec. VII, where preliminary results obtained for dimerized stack systems are reported.

Figure 7 puts in evidence one more point which has been overlooked in paper I, namely, the dependence of the χ_b^{-1} curves on ε_c. The reason for this rather subtle and unexpected interplay between interactions belonging to different symmetry representations can be understood in terms of the mf picture. To such aim, we make use of the asymmetry parameter ϕ defined in paper I as

$$\phi = \frac{2}{\mathcal{N}} \sum_{\substack{i \\ \text{odd}}} \frac{t_i - t_{i+1}}{t_i + t_{i+1}} = \mathcal{N}^{-3/2} \sum_\nu \sqrt{2\omega_\nu} g_\nu U_\nu \ . \tag{18}$$

In terms of ϕ the e-lph Hamiltonian [Eq. (14)] reads

$$\mathcal{H}_{ep} = -\mathcal{N}\sqrt{2}\phi \sum_i (-1)^i b_i \ ,$$

so that

$$\chi_b(\rho, \varepsilon_c) = -(\partial^2 \mathcal{E}_G / \partial \phi^2)_{\phi=0} \ .$$

However, this e-lph Hamiltonian has been derived by assuming that only the t_i's are modulated by the U_ν's. In the mf picture, if $\mathcal{E}_c \neq 0$, also z is actually modulated by the U_ν's via ρ [Eq. (4)]. The proper mf e-lph Hamiltonian, therefore, reads

$$\mathcal{H}_{ep}^{mf}=\mathcal{H}_{ep}-\phi^2\left[\frac{\partial^2 z}{\partial\phi^2}\right]_0\sum_i(-1)^i n_i\ , \tag{19}$$

where due to the symmetry of a regular chain in respect of positive or negative ϕ, the relation $(\partial z/\partial\phi)_0=0$ has been introduced. A little bit of algebra [based on Eqs. (4) and (6)] leads to

$$\left[\frac{\partial^2 z}{\partial\phi^2}\right]_0=\frac{\varepsilon_c}{1-\varepsilon_c(\partial\rho/\partial z)}\frac{\partial}{\partial z}\frac{\partial^2\mathcal{E}_G(z)}{\partial\phi^2}\ . \tag{20}$$

It is not difficult to realize that

$$\frac{\partial\rho}{\partial z}=-\frac{\partial^2\mathcal{E}_G(z)}{\partial z^2}$$

$$=\chi_v(\rho,\varepsilon_c=0)-\left[\frac{\partial^2\mathcal{E}_G(z)}{\partial\phi^2}\right]_0=\chi_b(\rho,\varepsilon_c=0)\ , \tag{21}$$

so that the second derivative of the ground-state energy in respect of ϕ gives

$$\chi_b(\rho,\varepsilon_c)=\chi_b(\rho,0)+(1-\rho)\frac{\varepsilon_c\chi_v(\rho,0)}{1-\varepsilon_c\chi_v(\rho,0)}\frac{\partial\chi_b(\rho,0)}{\partial\rho}\ . \tag{22}$$

The resulting $\chi_b^{-1}(\rho,\varepsilon_c)$ curves are reported in Fig. 7 as dashed lines, and compare well with the corresponding lr-Coul results (solid lines).

Equation (22) clearly shows that at the *N-I* interface, where $1-\varepsilon_c\chi_v(\rho,0)$ vanishes [Eq. (10)], $\chi_b\to\infty$ and the system becomes intrinsically unstable towards dimerization: *N-I* and dimerization instabilities are not independent. The physical meaning of Eqs. (19)–(22) is that the electronic energy gain due to dimerization increases if the charges on the molecular sites are allowed to reorganize in consequence of the dimerization, leading to a divergent behavior at the *N-I* interface.

The interplay found between Coul and *e*-lph interactions suggests investigating also the possible role of *e*-mv coupling in setting up the dimerization. To this aim the adiabatic *e*-mv Hamiltonian [Eq. (12)] has to be added to the purely electronic lr-Coul one [Eq. (1)]. As a consequence a new term

$$-\phi^2(\partial^2\rho/\partial\phi^2)_0\varepsilon_{sp}\sum_i(-1)^i n_i$$

adds to $\mathcal{H}_{ep}$. A treatment analogous to that reported in Eqs. (19)–(22) yields

$$\chi_b(\rho,\varepsilon_c,\varepsilon_{sp})=\chi_b(\rho,\varepsilon_c,0)+\frac{(1-\rho)\varepsilon_{sp}\chi_v(\rho,\varepsilon_c)}{1-\varepsilon_{sp}\chi_v(\rho,\varepsilon_c)}\times\frac{\partial\chi_b(\rho,\varepsilon_c,0)}{\partial\rho}\ . \tag{23}$$

Therefore, the χ_b^{-1} curves are further lowered by the effect of *e*-mv coupling, as shown in Fig. 8. Once more a divergence in χ_b occurs at the *N-I* interface where $\varepsilon_{sp}=\chi_v^{-1}(\rho,\varepsilon_c)$. The dimerization instability is affected not only by the Coul interactions, but also by the *e*-mv coupling, even if the Q_γ modes cannot directly interact with the U_ν ones due to their different symmetry. The lowering of the $\chi_b^{-1}(\rho)$ curves due to ε_{sp} clearly indicates that the *e*-mv coupling favors the dimerization, in agreement with early results obtained in one-electron models of segregated stack crystals.[27] The physical origin of such a lowering lies in the ionicity variation due to dimerization [$\chi_v(\rho,\varepsilon_c)(\partial/\partial\rho)\chi_b(\rho,\varepsilon_c,0)$ in Eq. (23) is equal to $\partial^2\rho/\partial\phi^2$]: If the molecules are consequently allowed to relax following the ionicity, the energy gain on dimerization increases. As in the case of the effect of ε_c on the dimerization, such a gain is very large at the *N-I* interface. A second result is worth noting: at the *N-I* interface the stack is intrinsically unstable towards dimerization even on the *N* side. This result appears now rather obvious: at ρ_N the system gives an infinite response to any perturbation (in this case the dimerization) able to induce ionicity variations.

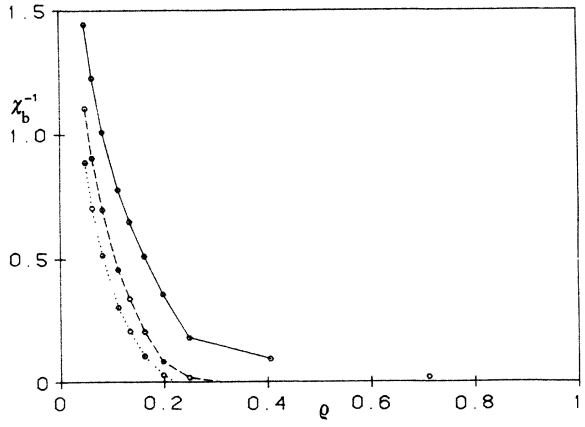

FIG. 8. Effect of ε_{sp} on the inverse of the electronic response to the *e*-lph perturbation for a system with $\varepsilon_c=1.8$ (lr-Coul calculations). Solid, dashed, and dotted lines refer to $\varepsilon_{sp}=0.0$, 1.0, and 2.0, respectively.

VI. ZERO-TEMPERATURE PHASE DIAGRAM

Before dealing with the complete phase diagram accounting for both *N-I* and *r-d* instabilities we briefly summarize the results so far reached for each of them. For what concerns the *N-I* interface, if ε_c and ε_{sp} are large enough, one finds a usual first-order phase transition, characterized by a bistability region (cf. Fig. 6), where the system can choose between two stable states with different ionicity, and, at the same time, cannot assume intermediate ionicity values. By lowering ε_c and ε_{sp} the instability range shrinks until it vanishes: the *N* and *I* phases merge. The *N-I* boundary can, therefore, be described as a first-order boundary with a critical point. As a matter of fact the *N* and *I* phases are conveniently distinguished in the entire parameters space. By remembering that the *N* and *I* phases are identified from a microscopic point of view as the phases with a nondegenerate and a degenerate ground state, respectively,[11] the *N-I* boundary can be continued beyond the critical point as the line separating intrinsically stable and unstable states towards dimerization.

The dimerization instability is characterized by a symmetry lowering driven by low-frequency lattice phonons and is expected to give rise to a continuous, second-order phase transition. It is easy to draw a parallel with the Peierls-type distortions usually observed in segregated stack systems.[28] As already discussed in the previous section, at the *N-I* interface the dimerization instability arises from the easy charge reorganization, or, in other words, from the "frictionless" motion of the electrons which follow the molecular displacements. In such conditions the dimerization is strictly analogous to the pure Peierls transition implying the translational degrees of freedom of the electrons. On the contrary when $\rho=1$, the dimerization instability, arising from degeneracy of the lowest A_1 and A_2 singlets which differ only in the spin distribution, can be easily assimilated to the spin Peierls instability. To put it in other terms at $\rho=1$ the system is analogous to a $U=\infty$ half-filled segregated stack: its charge and spin degrees of freedom are decoupled and the system can be described as an Heisenberg antiferromagnet. In between these two extremes both the charge and spin degrees of freedom will contribute to the instability giving rise to the so-called generalized Peierls instability.[28]

In order to understand what happens in a real system where both *N-I* and *r-d* instabilities coexist, one has to construct a complete phase diagram. This is done in Fig. 9 where, in the lower panel, the usual $\chi_b^{-1}(\rho,\varepsilon_c,\varepsilon_{sp})$ curve is drawn as a function of ρ for a system with $\varepsilon_c=1.8$, $\varepsilon_{sp}=1.3$. As we have already discussed, if one puts on the ordinate axis the ε_d values, this curve represents the boundary between stable ($\chi_b^{-1}>\varepsilon_d$) and unstable ($\chi_b^{-1}<\varepsilon_d$) states in respect to the dimerization. In the upper panel of the same figure we report the $z_0(\rho)$ curve calculated for the same values of ε_c and ε_{sp}. From this curve one can define the forbidden ρ region (in between ρ_N and ρ_I) and the bistability region (in between ρ_N^* and ρ_I^*). These two regions are then projected in the lower diagram which now represents a complete phase diagram. The shaded area indicates the forbidden ionicity region. In the *I* regime both in the bistability ($\rho_I<\rho<\rho_I^*$) and stability ($\rho>\rho_I^*$) ranges the regular stack cannot exist, being intrinsically unstable towards dimerization. In the *N* regime ($\rho<\rho_N$) instead, depending on the ε_d value, both regular or dimerized phases can be observed.

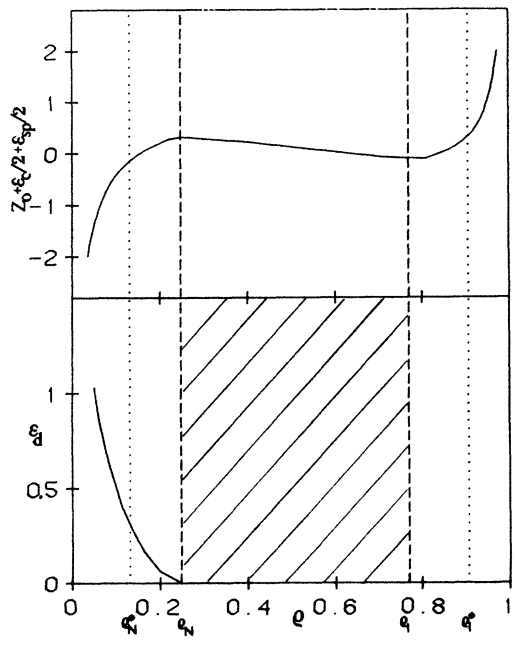

FIG. 9. Construction of the complete phase diagram for a mixed-stack CT crystal with $\varepsilon_c=1.8$ and $\varepsilon_{sp}=1.3$. The dashed area between ρ_N and ρ_I indicates the forbidden ρ region (for a regular chain); the areas between ρ_N and ρ_N^* and between ρ_I and ρ_I^* correspond to the bistability regions (see text).

In the *N* stable regime ($\rho<\rho_N^*$), if ε_d crosses the χ_b^{-1} curve one expects a pure dimerization transition: a second-order phase change from a neutral regular chain to a neutral dimerized one. At this point, however, one has to ask if the expression "neutral dimerized stack" has some physical meaning, i.e., if *N* and *I* phases can be distinguished in dimerized chains. It has in fact been recently claimed that "the charge transfer (i.e., the ionicity) is usually not a good quantity to distinguish the two phases,"[14] and that one has rather to rely on the degeneracy of the ground state. Since in dimerized chains the ground state is always nondegenerate, the *N-I* classification seems to become meaningless. However, mf calculations for a chain of isolated dimers, interacting only through the electrostatic potential,[29] actually indicate that if ε_c and ε_{sp} are large enough, the *N* and *I* phases are separated by a forbidden ρ region analogously to what occurs in regular stacks. The behavior of a dimerized chain will be obviously intermediate between that of the regular stack ($\phi=0$) and of the chain of isolated dimers ($\phi=1$), so that there is an $\varepsilon_c,\varepsilon_{sp}$ range where the *N-I* transition is a discontinuous, first-order one. The two phases are, therefore, distinguished on the basis of the quantitative difference in the ρ value, in much the same way as the liquid–vapor phases are usually distinguished. On the other hand, beyond the critical point the two phases merge, and they cannot be macroscopically distinguished anymore. However, it is convenient to keep the *N* and *I* classification by referring to a microscopic analysis analogous to that valid for regular stacks: *N* dimerized chains are those in which the fully ionic configurations do not contribute to the ground state, whereas *I* chains are those where no contribution of the fully neutral configuration to the ground state is found.

Another important observation concerns the variation of ionicity due to dimerization. The mf solution for the fully dimerized ($\phi=1$) chain indicates that the ionicity increases with ϕ and, at the same time, that the instability and bistability ranges become progressively narrower. Therefore, if the dimerization occurs in the regime of stability for the *N* stack ($\rho<\rho_N^*$) the corresponding dimer will have a greater charge but will be always in a ρ stability region. In particular if ε_c and ε_{sp} are large enough to give rise to a forbidden ρ region also in the dimerized chain, the dimer will be in the *N* side. In conclusion, for $\rho<\rho_N^*$ at $\varepsilon_d=\chi_b^{-1}$ one expects a second-order dimerization instability. As a final observation, we remark that

due to the charge and nuclear relaxation, the energy of the dimerized states might lower, giving rise to a three-minima potential. Accordingly, one could observe a slightly first-order dimerization, occurring before the setting up of the second-order phase change.[30]

Let us now briefly investigate the phase transition when the crossing $\varepsilon_d = \chi_b^{-1}$ occurs in the N bistability region ($\rho_N^* < \rho < \rho_N$). In such a region two stable states are available to the regular chain, a N and an I one. At ρ_N^* the N state has the lower energy, but the energy difference between the two states lowers by increasing ρ, until it vanishes at a point which could be evaluated through the Maxwell equal area rule;[26] after this point, until ρ_N, the I state has the lower energy. Depending on the external "noise" (i.e., the temperature, the defect concentration, and other experimental conditions) the N-I transition will occur when the two states have the same energy (Maxwell convention) or at ρ_N, where the N state becomes unstable (delay convention).[31] By adopting the Maxwell convention one could say that if ε_d crosses the χ_b^{-1} curve before the vanishing of the N-I energy difference, a second-order dimerization transition will occur. However, this statement is not correct: the I state is, in fact, unstable towards dimerization, and, therefore, one actually has to consider a three-minima potential. If the dimerization makes the energy of the I states lower than that of the N one before the onset of the second-order phase transition, one will observe a first-order phase change[30] from a neutral regular stack to an ionic dimerized one. Of course this is also the kind of transition expected if ε_d crosses the χ_b^{-1} curve when the I state has lower energy than the N one. However, if the noise is low, also N metastable states can be reached (delay convention), and one could also observe a soft mode. In general, it is difficult to precisely state the evolution of the phase transition; however, the presence of many (at least three) different equilibrium positions (minima in the energy curve) with comparable energy values strongly points towards a first-order phase change, very sensitive to the external conditions and characterized by the coexistence of different phases.

VII. COMPARISON WITH REAL SYSTEMS

A very large number of quasi-one-dimensional mixed-stack CT crystals is known, and the great majority of them is characterized by a regular stack and low-ionicity values ($\rho \lesssim 0.3$).[21,32] As far as we know, only two systems exhibit intermediate ionicities ($0.3 \lesssim \rho \lesssim 0.7$), and both have a dimerized stack structure.[16,33] Finally, the few CT crystals lying in the high-ionicity region are characterized by a regular stack structure at 300 K.[16]

Apart from the well-known case of TTF-CA,[4-6] which will be discussed below, in general the temperature does not induce phase transitions in systems with low or intermediate ionicity (we are not concerned here with disorder-order or orientational phase transitions). On the other hand, by lowering temperature the highly ionic compounds undergo an *r-d* stack transition without remarkable ionicity variation.[11,16]

This general behavior can be understood on the basis of the above described 0 K phase diagram. The analysis of optical data of several CT crystals allows one to estimate the variability ranges of the various parameters occurring in the phase diagram (Refs. 13 and 21): $1.0 \lesssim \varepsilon_c \lesssim 2.0$; $0.5 \lesssim \varepsilon_{sp} \lesssim 1.5$; $0.05 \lesssim \varepsilon_d \lesssim 0.25$. On the basis of these data, Figs. 7 and 8 clearly show that low-ionicity CT crystals are indeed expected to exhibit a regular-stack structure at all temperatures, whereas ionic systems will always be dimerized at sufficiently low temperatures. On the other hand, Fig. 5 indicates that intermediate ionicity systems are very unlikely to be found due to the presence of forbidden ionicity ranges (we remind that such ionicity gaps may occur also in dimerized stack systems).

The reason why intermediate ionicity CT crystals are already dimerized at 300 K, whereas the highly ionic ones dimerize only at low temperatures, can be qualitatively understood as follows. In the previous section we have discussed how near the N-I interface the *r-d* stack instability is analogous to a pure Peierls instability, whereas for $\rho \sim 1$ it can be assimilated to a spin-Peierls one. It is well known that the first kind of instability involves a much larger energy gain than the second one, so that the transition temperature is expected to be higher in the pure Peierls than in the spin-Peierls transition.[28]

In order to give a sounder basis to the above statement, we have performed calculations on dimerized stacks to evaluate, for a given ε_d, the equilibrium position of the distorted system and the consequent energy gain. We have considered both an uncorrelated system ($\varepsilon_c = 0$) and, via lr-Coul calculations, a correlated one ($\varepsilon_c = 1.8$); in any case we have assumed $\varepsilon_{sp} = 0$, $\varepsilon_d = 0.15$. The results are shown in Fig. 10, where in the upper panels we give, as a measure of the equilibrium dimerization, the corresponding ϕ, whereas in the lower panels the energy gain (ΔE) on dimerization is reported. Left and right sides refer to the $\varepsilon_c = 0$ and to the $\varepsilon_c = 1.8$ results, respectively. For each ε_c value, both ϕ and ΔE are at a maximum near the N-I boundary, and rapidly decrease on N side. On the I side the decrease is slower, and ϕ and ΔE vanish only at $\rho = 1$. The ΔE decrease on the I side clearly indicates that the dimerization temperature of ionic mixed-stack crystals will progressively lower by increasing ρ towards 1, in good agreement with experimental observations.[33]

Now we turn the attention to the TTF-CA system, the only one known to undergo a *Nr-Id* phase transition by lowering the temperature or by increasing the pressure.[4-6] The microscopic parameters characterizing TTF-CA at 300 K have been evaluated as $\varepsilon_c \sim 1.8$, $\varepsilon_{sp} \sim 1.3$, and $\varepsilon_d \sim 0.1$–0.2 ($t = 0.21$ eV).[34] Since temperature and pressure cause a lattice contraction before the transition,[35] t presumably increases, thus decreasing ε_c and ε_{sp}. Considering also the uncertainty in the parameters estimate, the TTF-CA phase diagram is probably in between those reported in Figs. 9 and 11. The ionicity of the crystal varies between 0.2 and 0.3 before the phase transition;[6,16] in any case the system lies in the bistability region. Thus it is very difficult to precisely state the evolution of the phase transition: we can say that it is most probably a first-order one and that it will be very sensitive

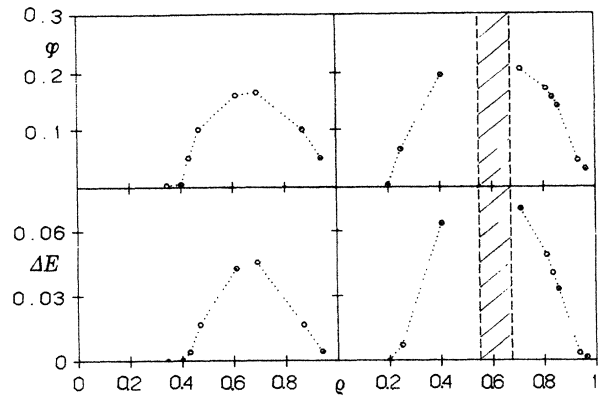

FIG. 10. Extent of dimerization (expressed by the asymmetry parameter ϕ) and electronic energy gain upon dimerization (ΔE) as functions of ρ. Left panels: $\varepsilon_c = 0.0$; right panels: $\varepsilon_c = 1.8$; $\varepsilon_d = 0.15$ and $\varepsilon_{sp} = 0.0$ always.

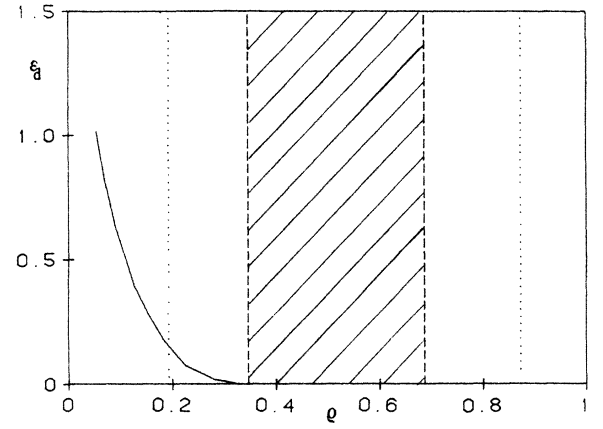

FIG. 11. Phase diagram for a mixed-stack CT crystal with $\varepsilon_c = 1.4$ and $\varepsilon_{sp} = 1.1$.

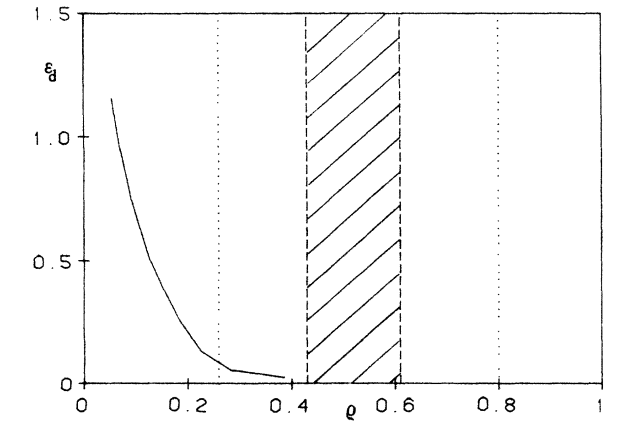

FIG. 12. Phase diagram for a mixed-stack CT crystal with $\varepsilon_c = 1.4$ and $\varepsilon_{sp} = 0.6$ (e.g., DBTTF-TCNQ).

to the experimental conditions (purity of the crystal, defects, temperature, etc.). It is then no more surprising to find differences between the results obtained in various laboratories or to observe a different evolution of temperature- and pressure-induced phase transitions.[4-6] On the basis of Figs. 9 and 11 phase diagrams, one would expect the ionicity of the *Id* phase to be between 0.7 and 0.8, somewhat larger than that experimentally observed. However, this ρ value is relevant to the regular stack; calculations performed on the fully dimerized chain indicate that on the *I* side the ionicity tends to decrease with the dimerization.

It is instructive to compare the TTF-CA phase diagram with that of dibenzotetrathiafulvalene-tetracyanoquinodimethane (DBTTF-TCNQ), a crystal which under pressure undergoes a different kind of phase transition, *Nr-Nd* (ρ varies from 0.2 to ~ 0.4).[15] At ambient pressure the microscopic parameters of DBTTF-TCNQ have been estimated as $\varepsilon_c \sim 1.4$, $\varepsilon_{sp} \sim 0.6$, $\varepsilon_d \sim 0.1-0.2$.[34] The corresponding phase diagram is reported in Fig. 12. Due to the low ε_c and ε_{sp} values, the system is stable in respect to the *N-I* transition: a slight increase in ρ induced by the pressure will cause a crossing of the *r-d* instability curve before reaching the bistability region. A pure (probably second-order) dimerization transition is expected, accompanied by a slight increase of ρ, in agreement with the available preliminary experimental data.[15]

VIII. CONCLUSIONS

In the present paper we have investigated the ground-state properties of mixed-regular-stack CT organic solids. VB calculations have allowed us to deal with a quite complete model where the electron-electron and electron-phonon interactions, required to achieve a realistic description of these systems, are accounted for. The on-site electronic interactions, which are at least one order of magnitude greater than the other energies relevant to the problem, have been assumed infinite by excluding from the beginning the states with doubly ionized sites. The intersite electrostatic interactions have been introduced as a sum of unscreened Coulomb interactions between point charges at the molecular sites. In any case, the results seem not to be strongly dependent on the explicit form of the electrostatic potential, as they generally compare well with those obtained in mf approximation. A perturbative, adiabatic approach on the basis of the electronic correlated functions has then been adopted to account for the effects of both *e*-lph and *e*-mv couplings. This allows us to get a first sound understanding of the subtle competitive-cooperative interplay between the various parameters of the theory in setting up the *N-I* and dimerization instabilities.

The four-dimensional zero-temperature phase diagram which results from the model predicts the occurrence of only three stable phases: *Nr*, *Nd*, and *Id*. The *Ir* phase is not found since the *N-I* boundary actually coincides with the line where the regular chain becomes intrinsically unstable towards dimerization due to the degeneracy of the ground state. In spite of this coincidence, the *N-I* bound-

ary retains a physical meaning of its own: it corresponds in fact to a first-order boundary with a critical point. This is a remarkable observation since it holds also for dimerized stacks and, therefore, allows us to make a physically meaningful distinction between N and I dimerized chains, even if their ground states are always nondegenerate.

In addition to investigating the stability ranges of the various phases, the proposed phase diagram can also be analyzed to gain insight into the nature of the various phase transitions observed in mixed-stack CT crystals. In particular, we have found that dimerization transitions starting from the N side may occur; they are likely second order, and in general imply a small-ionicity increase. On the contrary the N-I (actually Nr-Id) phase transitions are most likely first order and are expected to be very sensitive to the experimental conditions. Moreover, the requirements for the occurrence of a N-I phase transition appear rather stringent, as a subtle balance of the various parameters is needed to drive the systems into the N-I bistability range. It is then not surprising that TTF-CA is to date the only CT crystal confirmed to undergo such a kind of phase change. Finally, calculations of the energy gain upon dimerization support the interpretation of the dimerization transition observed in ionic mixed-stack CT crystals as a Peierls-type one: a pure Peierls near the N-I boundary which turns to a spin Peierls as $\rho \rightarrow 1$.

Refinements of the present model would imply the inclusion of the interchain electrostatic interactions, which are responsible for the largest interchain coupling,[36] and the relaxation of the adiabatic approximation introduced in dealing with the phonons. Moreover the model has been worked out for a perfect crystal, so that neither the structure of defects, nor their possible role in setting up the instabilities has been investigated. We believe, however, that the model in its present form is quite adequate in offering a comprehensive and general view of the phase diagram of mixed-stack CT crystals.

ACKNOWLEDGMENTS

We thank Z. G. Soos for giving us the original version of his VB computer program and for the stimulating discussion and correspondence. We also acknowledge the helpful discussions with Y. Fukuyama and N. Nagaosa, as well as the continuous encouragement of C. Pecile. This work has been supported by the Ministero della Pubblica Istruzione of Italy. One of us (A.P.) would like to thank the International Conference on the Physics and Chemistry of Low-Dimensional Synthetic Metal (ICSM84) for financial support.

[1]Z. G. Soos and D. J. Klein, in *Molecular Association,* edited by R. Foster (Academic, New York, 1975), Vol. 1, p. 1.

[2]J. B. Torrance, J. E. Vazquez, J. J. Mayerle, and V. Y. Lee, Phys. Rev. Lett. **46**, 253 (1981).

[3]J. B. Torrance, A. Girlando, J. J. Mayerle, J. C. Crowley, V. Y. Lee, P. Batail, and S. J. LaPlaca, Phys. Rev. Lett. **47**, 1747 (1981).

[4]A. Girlando, F. Marzola, and C. Pecile, J. Chem. Phys. **79**, 1075 (1983).

[5]Y. Tokura, Y. Kaneko, H. Okamoto, S. Tanuma, T. Koda, T. Mitani, and G. Saito, Mol. Cryst. Liq. Cryst. **125**, 71 (1985).

[6]Y. Tokura, H. Okamoto, T. Mitani, G. Saito, and T. Koda, Solid State Commun. **57**, 607 (1986); A. Girlando, C. Pecile, A. Brillante, and K. Syassen, *ibid.* **57**, 891 (1986).

[7]J. Hubbard and J. B. Torrance, Phys. Rev. Lett. **47**, 1750 (1981); R. Bruinsma, P. Bak, and J. B. Torrance, Phys. Rev. B **27**, 456 (1983).

[8]M. Avignon, C. A. Balseiro, C. R. Proetto, and B. Alascio, Phys. Rev. B **33**, 205 (1986).

[9]Z. G. Soos and S. Kuwajima, Chem. Phys. Lett. **122**, 315 (1985); Z. G. Soos, S. Kuwajima, and R. H. Harding, J. Chem. Phys. **85**, 601 (1986).

[10]T. Luty and B. Kuchta, Phys. Rev. B **35**, 8542 (1987).

[11]A. Girlando and A. Painelli, Phys. Rev. B **34**, 2131 (1986).

[12]N. Nagaosa and J. Takimoto, J. Phys. Soc. Jpn. **55**, 2737 (1986); **55**, 2747 (1986); N. Nagaosa, *ibid.* **55**, 2756 (1986).

[13]A. Girlando and A. Painelli, Physica **143B**, 559 (1986).

[14]B. Horovitz and J. Solyom, Phys. Rev. B **35**, 7081 (1987).

[15]A. Girlando, C. Pecile, A. Brillante, and K. Syassen, Synth. Met. **19**, 503 (1987).

[16]A. Girlando, A. Painelli, and C. Pecile, Mol. Cryst. Liq. Cryst. **120**, 17 (1985).

[17]Due to the spin degrees of freedom the homogeneous distribution does not correspond to $\rho=0.5$ but to a higher value $\rho \sim 0.6$ (Ref. 11).

[18]Z. G. Soos and S. Ramashesa, Phys. Rev. B **29**, 5410 (1984); S. Ramashesa and Z. G. Soos, J. Chem. Phys. **80**, 3278 (1984); Int. J. Quantum. Chem. **25**, 1003 (1984).

[19]Z. G. Soos, R. H. Harding, and S. Ramashesa, Mol. Cryst. Liq. Cryst. **125**, 59 (1985).

[20]K. Kral, J. Malek, and B. Hejda, Chem. Phys. **45**, 101 (1980); J. Ladik, A. Karpfen, G. Stollhoff, and P. Fulda, *ibid.* **7**, 267 (1975); S. Millefiori and A. Millefiori, J. Mol. Struc. **104**, 131 (1983).

[21]A. Painelli and A. Girlando, J. Chem. Phys. **87**, 1705 (1987).

[22]J. Hubbard, Phys. Rev. B **17**, 494 (1978); S. Mazumdar and S. N. Dixit, *ibid.* **34**, 3683 (1986).

[23]S. Mazumdar and Z. G. Soos, Phys. Rev. B **18**, 1991 (1978).

[24]H. M. McConnell, B. M. Hoffmann, and R. M. Metzger, Proc. Natl. Acad. Sci. U.S.A. **53**, 46 (1965).

[25]A. Painelli and A. Girlando, J. Chem. Phys. **84**, 5665 (1986).

[26]D. Landau and E. M. Lifshitz, *Statistical Physics* (Addison-Wesley, Reading, MA, 1969).

[27]M. J. Rice, C. B. Duke, and N. O. Lipari, Solid State Commun. **17**, 1089 (1975); M. J. Rice (private communication).

[28]J. W. Bray, L. V. Interrante, I. S. Jacobs, and J. C. Bonner, in *Extended Linear Chain Compounds,* edited by J. S. Miller (Plenum, New York, 1983), Vol. 3, Chap. 7.

[29]Z. G. Soos, H. J. Keller, W. Moroni, and D. Nothe, Ann. N.Y. Acad. Sci. **313**, 442 (1978). The extension of the model for the analysis discussed in present paper is straightfoward and therefore not reported.

[30]P. W. Anderson, *Basic Notions in Condensed Matter Physics* (Benjamin, Menlo Park, CA, 1984), Chap. 2.

[31]G. Venkataraman and V. Balakrishnan, in *Synergetics and Dynamical Instabilities,* Proceedings of the International

School of Physics, "Enrico Fermi," 99th Course, edited by G. Caglioti and H. Haken (North-Holland, Amsterdam, in press).

[32]F. H. Herbstein, in *Perspective in Structural Chemistry,* edited by J. P. Dunitz and J. A. Ibers (Wiley, New York, 1971), Vol. 4, p. 166.

[33]A. Girlando, A. Painelli, and C. Pecile, J. Chem. Phys. (to be published).

[34]A. Painelli and A. Girlando, Synth. Met. **19**, 509 (1987).

[35]R. M. Metzger and J. B. Torrance, J. Am. Chem. Soc. **107**, 117 (1985).

[36]S. Kuwajima and Z. G. Soos, Synth. Met. **19**, 489 (1987).